

Assessment of CO₂ adsorption capacity on activated carbons by a combination of batch and dynamic tests

Marco Balsamo, Ana Silvestre-Albero, Joaquin Silvestre-Albero,
Alessandro Erto, Francisco Rodriguez-Reinoso, and Amedeo Lancia

Langmuir, **Just Accepted Manuscript** • DOI: 10.1021/la500780h • Publication Date (Web): 30 Apr 2014

Downloaded from <http://pubs.acs.org> on May 6, 2014

Just Accepted

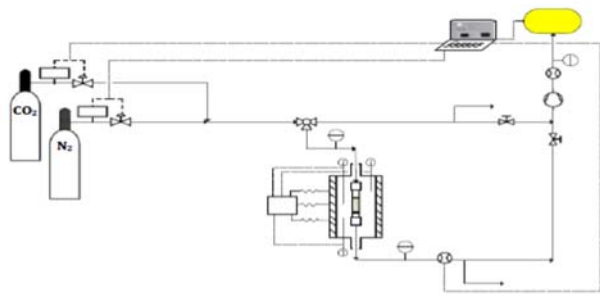
“Just Accepted” manuscripts have been peer-reviewed and accepted for publication. They are posted online prior to technical editing, formatting for publication and author proofing. The American Chemical Society provides “Just Accepted” as a free service to the research community to expedite the dissemination of scientific material as soon as possible after acceptance. “Just Accepted” manuscripts appear in full in PDF format accompanied by an HTML abstract. “Just Accepted” manuscripts have been fully peer reviewed, but should not be considered the official version of record. They are accessible to all readers and citable by the Digital Object Identifier (DOI®). “Just Accepted” is an optional service offered to authors. Therefore, the “Just Accepted” Web site may not include all articles that will be published in the journal. After a manuscript is technically edited and formatted, it will be removed from the “Just Accepted” Web site and published as an ASAP article. Note that technical editing may introduce minor changes to the manuscript text and/or graphics which could affect content, and all legal disclaimers and ethical guidelines that apply to the journal pertain. ACS cannot be held responsible for errors or consequences arising from the use of information contained in these “Just Accepted” manuscripts.



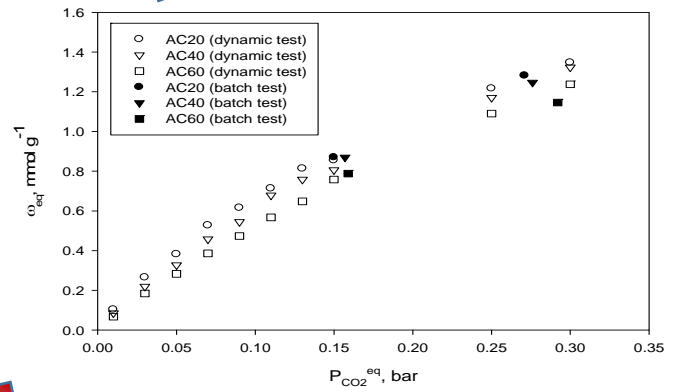
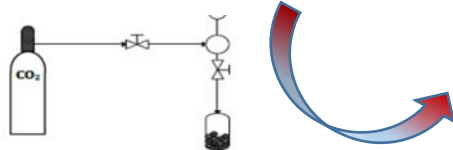
1
2
3
4
5
6
7
8
9
10
11
12
13
14
15
16
17
18
19
20
21
22
23
24
25
26
27
28
29
30
31
32
33
34
35
36
37
38
39
40
41
42
43
44
45
46
47
48
49
50
51
52
53
54
55
56
57
58
59
60

Graphical Abstract

Dynamic CO₂ adsorption apparatus



Batch CO₂ adsorption apparatus



CO₂ adsorption isotherms on AC samples

1
2
3
4 1 Assessment of CO₂ adsorption capacity on activated
5
6
7
8 2 carbons by a combination of batch and dynamic tests
9
10

11
12 3 *Marco Balsamo*¹, *Ana Silvestre-Albero*², *Joaquín Silvestre-Albero*², *Alessandro*
13
14 4 *Erto*^{1*}, *Francisco Rodríguez-Reinoso*², *Amedeo Lancia*¹
15
16
17
18 5

19
20 6 ¹ Dipartimento di Ingegneria Chimica, dei Materiali e della Produzione Industriale, Università
21
22 7 degli Studi di Napoli Federico II, Piazzale Vincenzo Tecchio 80, 80125 Napoli, Italy
23
24

25 8 ² Laboratorio de Materiales Avanzados, Departamento de Química Inorgánica, Instituto
26
27 9 Universitario de Materiales, Universidad de Alicante, Ap. 99, E-03080 Alicante, Spain
30
31 10

32
33 11 **Abstract**

34
35 12 In this work, batch and dynamic adsorption tests are coupled for an accurate evaluation of CO₂
36
37 13 adsorption performance for three different activated carbons obtained from olives stones by
38
39 14 chemical activation followed by physical activation with CO₂ at varying times, i.e. 20, 40 and 60
40
41 15 h. Kinetic and thermodynamic CO₂ adsorption tests from simulated flue-gas at different
42
43 16 temperature and CO₂ pressure are carried out both in batch (a manometric equipment operating
44
45 17 with pure CO₂) and dynamic (a lab-scale fixed-bed column operating with CO₂/N₂ mixture)
46
47 18 conditions. The textural characterization of the activated carbon samples shows a direct
48
49 19 dependence of both micropore and ultramicropore volume on the activation time, hence AC60
50
51
52
53
54
55

56
57 * Corresponding author. Tel.: +39 081 7682236; fax: +39 081 5936936.
58 *E-mail address:* aleserto@unina.it (A. Erto).
59
60

1
2
3 20 has the higher contribution. The adsorption tests conducted at 273 and 293 K showed that, when
4
5 21 CO₂ pressure is lower than 0.3 bar, the lower the activation time the higher CO₂ adsorption
6
7 22 capacity and a ranking $\omega_{\text{eq}}(\text{AC20}) > \omega_{\text{eq}}(\text{AC40}) > \omega_{\text{eq}}(\text{AC60})$ can be exactly defined when T= 293
8
9 23 K. This result can be likely ascribed to a narrower pore size distribution of the AC20 sample,
10
11 24 whose smaller pores are more effective for CO₂ capture at higher temperature and lower CO₂
12
13 25 pressure, the latter representing operating conditions of major interest for decarbonation of a
14
15 26 flue-gas effluent. Moreover, the experimental results obtained from dynamic tests confirm the
16
17 27 results derived from the batch tests in terms of CO₂ adsorption capacity. It is important to
18
19 28 highlight that the adsorption of N₂ on the synthesized AC samples can be considered negligible.
20
21 29 Finally, the importance of a proper analysis of characterization data and adsorption experimental
22
23 30 results is highlighted for a correct assessment of CO₂ removal performances of activated carbons
24
25 31 at different CO₂ pressure and operating temperature.
26
27
28
29
30
31
32

33 **Keywords:** CO₂; adsorption; activated carbon; carbon capture and storage; global warming
34
35
36
37
38

39 1. Introduction

40
41 36 CO₂ is unanimously considered as the primary greenhouse gas emitted through human
42
43 37 activities, responsible for about 60% of increased greenhouse effect and climate change^{1,2}. The
44
45 38 combustion of fossil fuels for the generation of heat and power energy is the main CO₂ emission
46
47 39 source. Although many efforts are currently devoted to develop new and cleaner technologies,
48
49 40 such as chemical looping combustion, new gasification technologies for power plants and
50
51 41 hydrogen-based fuel cells^{2,3}, an immediate and effective CO₂ mitigation can be pursued by the
52
53 42 adoption of appropriate post combustion technologies. The use of porous solids for CO₂ capture
54
55
56
57
58
59
60

1
2
3 43 is gaining crescent interest within the Carbon Capture and Storage (CCS) strategy aimed at a
4
5
6 44 short-term reduction of CO₂ industrial emissions. Currently, several techniques are applied for
7
8 45 the separation and capture of CO₂, which include amine-based absorption, membrane separation,
9
10 46 cryogenic distillation and adsorption process⁴⁻⁶. An appropriate CO₂ capture technology should
11
12 47 be effective, low cost, environmentally benign and easily applicable. In this context, adsorption
13
14 48 technology represents a promising solution, which can be easily implemented in existing power
15
16 49 plants. Moreover, it is a well-established technique which can be adopted for the removal of
17
18 50 different classes of pollutants from both gaseous and liquid streams, thanks to a high versatility
19
20 51 and general low maintenance costs⁷⁻¹². Although different classes of adsorbents are extensively
21
22 52 investigated in the pertinent literature, the use of activated carbons (ACs) for CO₂ capture has a
23
24 53 great appeal thanks to their tuneable porous structure, a wide adsorption spectrum and relatively
25
26 54 limited costs^{7,8,13,14}. In addition, CO₂ adsorption on ACs has been demonstrated to be a reversible
27
28 55 process, hence CO₂ recovery and AC regeneration can be simultaneously pursued by a
29
30 56 desorption process¹⁵⁻¹⁸.

31
32
33
34
35
36 57 Activated carbons can be manufactured starting from various carbonaceous precursors^{17,19-}
37
38 58 ²¹. In particular, lignocellulosic materials are characterized by general low-costs and abundant
39
40 59 availability, which can allow a significant saving in adsorbent production and process
41
42 60 management. Many efforts have been expended in the development of adsorbent materials from
43
44 61 agricultural wastes²¹⁻²⁵ and, specifically, to define the optimal textural as well as chemical
45
46 62 properties to maximize CO₂ capture²⁶⁻²⁸. At the current state-of-the-art, there is a general
47
48 63 accordance in the literature to consider the increase in CO₂ adsorption capacity, under flue-gas
49
50 64 simulated conditions (CO₂ partial pressure typically lower than 0.15 bar), as closely related to a
51
52 65 high total or micropore volume coupled with a narrower micropore size distribution shifted
53
54
55
56
57
58
59
60

1
2
3 66 towards ultramicropores^{13,26,29-31}. In particular, Sun and co-workers²⁹ elucidated the main
4
5 67 functional dependencies by a dedicated statistical analysis applied to a large set of activated
6
7
8 68 carbons, in which the correlation degree between CO₂ adsorption capacity and textural properties
9
10 69 was determined. Similarly, Yin and co-workers³¹ analysed a large number of experimental works
11
12 70 present in the literature and concluded that the surface area of activated carbon is not the
13
14 71 determining factor for CO₂ adsorption, while ultramicropores have a significant influence.

15
16
17 72 On the other side, Balsamo and co-workers³² pointed out that micropore diffusion is the
18
19 73 limiting step of adsorption process carried out in fixed-bed column. Simultaneously, they
20
21 74 highlighted the positive effect exerted by mesopores in the enhancement of CO₂ adsorption rate,
22
23 75 as already stated by different authors, which worked with volumetric (manometric) apparatuses
24
25 76 operated in batch mode^{11,29}.

26
27
28
29 77 Despite the large number of studies focused on the determination of the correlations
30
31 78 between activated carbon properties and CO₂ capture performances, few studies are performed in
32
33 79 simulated flue-gas streams^{15,17,29,32}. In addition, the current literature is still lacking of thorough
34
35 80 studies on CO₂ adsorption onto activated carbons in dynamic conditions, as most of the
36
37 81 experimental works are carried out in volumetric/gravimetric apparatuses. Even less studies are
38
39 82 available in which the adsorption of CO₂ is investigated simultaneously from simulated flue-gas,
40
41 83 in dynamic systems, and as a function of the main operational parameters (e.g. gas temperature,
42
43 84 CO₂ concentration, etc.)³³⁻³⁵.

44
45
46
47
48 85 The goal of this work is an experimental analysis of CO₂ adsorption onto activated carbons
49
50 86 (AC), produced starting from olive stones, through a combined set of batch and dynamic tests. A
51
52 87 microstructural characterization of the AC samples by N₂ and CO₂ adsorption was carried out
53
54 88 aimed at assessing the contribution of mesopores, micropores and narrow micropores. Kinetic
55
56
57
58
59
60

1
2
3 89 and thermodynamic CO₂ adsorption tests at different CO₂ pressure and temperature were
4
5 90 performed both in batch (glass-made manometric adsorption equipment operating with pure
6
7
8 91 CO₂) and in dynamic (a lab-scale fixed-bed column operating with CO₂/N₂ mixture) conditions,
9
10 92 for a thorough comparison. The complementarity of batch and dynamic experiments was
11
12 93 highlighted in order to pursue a correct determination of CO₂ adsorption capacity and to assess
13
14 94 the factors affecting the CO₂ capture in operating conditions typical of a flue-gas (in terms of
15
16 95 temperature and CO₂ concentration).
17
18
19
20 96

22 97 **2. Materials and methods**

23 98 *2.1. Activated carbon samples*

24
25 99 Three AC samples were synthesized starting from the same lignocellulosic precursor (i.e. olive
26
27 100 stones) according to the procedure reported by Silvestre-Albero and co-workers³⁶. A
28
29 101 combination of chemical and physical activation processes was adopted which involved the
30
31 102 impregnation with an aqueous solution of ZnCl₂ at 358 K and a heat treatment under a N₂ flow at
32
33 103 773 K; this was followed by a physical activation performed with CO₂ (100 cm³ min⁻¹) at 1098 K
34
35 104 using different periods of time, i.e. 20, 40 and 60 h, which gave rise to the different labelled
36
37 105 materials (i.e. AC20, AC40 and AC60, respectively).
38
39
40
41
42

43 106 A particle size range 1.00-2.36 mm was selected for all the experimental runs by mechanical
44
45 107 sieving.

46
47 108 The textural properties of the synthesized AC samples were determined in a fully automated
48
49 109 manometric equipment, the N₂Gsorb-6 porosimeter (www.g2mtech.com). Adsorption isotherms
50
51 110 of N₂ and CO₂ were obtained at 77 K and 273 K, respectively. Before each experiment, the
52
53 111 samples were outgassed at 423 K for 4 h under vacuum (10⁻⁸ bar) in order to remove humidity.
54
55
56
57
58
59
60

1
2
3 112 The main microstructural parameters of the AC samples were obtained from mathematical
4
5 113 processing of N₂ and CO₂ adsorption isotherms according to the models commonly applied in the
6
7
8 114 literature. In particular, the “apparent” surface area was obtained using the BET method. The
9
10 115 micropore volume (V_o) was deduced from the N₂ adsorption data using the Dubinin–
11
12 116 Raduskevitch (DR) equation, while the mesopore volume (V_{meso}) was obtained as the difference
13
14 117 between the total pore volume (V_t) adsorbed at $P/P^0 \sim 0.95$ and the micropore volume (V_o). The
15
16 118 pore volume corresponding to the narrow microporosity (V_n) was obtained after application of
17
18 119 the DR equation to the CO₂ adsorption data at 273 K.
19
20
21
22 120
23

24 121 *2.2 Kinetic batch adsorption experiments*

25
26
27 122 Pure CO₂ batch adsorption kinetics on the AC samples was carried out at 293 K in a glass-made
28
29 123 manometric adsorption equipment developed by the Laboratorio de Materiales Avanzados group.
30
31 124 Experimental runs were performed at two different initial CO₂ pressures, namely 0.25 and 0.42
32
33 125 bar and employing 0.2 g of each AC tested. The adsorption kinetics was determined from the
34
35 126 pressure decrease in the pressure transducer with time. Prior to the adsorption experiment, the
36
37 127 sample was degassed under vacuum (10^{-7} bar) at 423 K for 4 h.
38
39
40
41 128
42

43 129 *2.3. Dynamic adsorption experiments*

44
45
46 130 The dynamic adsorption runs were carried out in a lab-scale fixed-bed column (length=0.13 m;
47
48 131 inner diameter=0.02 m) made up of Pyrex glass. The fixed bed temperature was controlled by
49
50 132 means of cylindrical shell Watlow band heaters, enveloped in a thermal insulating layer of
51
52 133 ceramic fibres, and connected to EZ-PM® PID controllers (Watlow).
53
54
55
56
57
58
59
60

1
2
3 134 Two mass flow controllers (series El Flow Bronkhorst 201-CV) were used to generate a gas
4
5 135 (N₂+CO₂) with 1-30% CO₂ concentration. Gas volumetric flow rate variations, occurring in the
6
7
8 136 fixed bed as a consequence of CO₂ adsorption, were monitored by means of a mass flow meter
9
10 137 series El Flow Bronkhorst 201-CV placed at the exit of the adsorption column.
11
12 138 A continuous NDIR (non-dispersive infrared) gas analyzer (AO2020 Uras 26 model provided by
13
14 139 ABB) was adopted for the determination of CO₂ concentration. Finally, data acquisition and
15
16 140 elaboration were performed by interfacing the analyser with a PC unit via LabView™ software.
17
18 141 Experimental tests in fixed-bed column were carried out by feeding the column, charged with a
19
20 142 fixed adsorbent amount (i.e. 0.015 kg), with a 1.5 L min⁻¹ gas stream (N₂+CO₂) at 293 K and 1
21
22 143 atm total gas pressure.
23
24
25
26

27 144 CO₂ dynamic adsorption results were processed to obtain the corresponding adsorption
28
29 145 isotherms. As known, the material balance on CO₂ over the fixed-bed column leads to the
30
31 146 determination of the equilibrium CO₂ adsorbed amount, ω_{eq} [mmol g⁻¹]:
32
33

$$\omega_{\text{eq}} = \frac{Q_{\text{CO}_2}^{\text{in}} \rho_{\text{CO}_2}}{m M_{\text{CO}_2}} \int_0^{t_{\text{eq}}} \left(1 - \frac{Q_{\text{CO}_2}^{\text{out}}(t)}{Q_{\text{CO}_2}^{\text{in}}} \right) dt \quad (1)$$

34
35
36 147
37
38
39 148 where $Q_{\text{CO}_2}^{\text{in}}$ and $Q_{\text{CO}_2}^{\text{out}}$ are column inlet and outlet CO₂ volumetric flow rates, respectively; m is the
40
41
42 149 mass of adsorbent; ρ_{CO_2} [mg L⁻¹] represents CO₂ density (evaluated at 293 K and 1 bar); M_{CO_2} is
43
44 150 its molecular weight [mg mmol⁻¹].
45
46

47 151 A check on adsorption capacity was carried by desorption runs on spent AC samples. Pure N₂
48
49 152 was used as desorbing agent and the CO₂ outlet concentration was monitored by means of the
50
51 153 NDIR analyzer. The desorption profiles were elaborated to obtain the total specific amount of
52
53 154 CO₂ desorbed from the spent AC, ω_{des} [mmol g⁻¹], through a material balance, similar to Eq. (1):
54
55
56
57
58
59
60

$$\omega^{\text{des}} = \frac{\rho_{\text{CO}_2}}{mM_{\text{CO}_2}} \int_0^{t_{0.1}} Q_{\text{CO}_2}^{\text{out}}(t) dt \quad (2)$$

156 in which $t_{0.1}$ is the time required to complete the desorption process, assumed as the one
157 corresponding to the NDIR low detection limit (0.1% CO₂ by vol.). The maximum allowed
158 discrepancy between ω_{eq} and ω_{des} was set at 5 %.

159 Further details about dynamic experimental apparatus and adsorption tests were reported in
160 a previous work¹⁷.

161

162 **3. Results and discussion**

163 *3.1. Activated carbon textural characterization*

164 The characterization of the textural properties of the AC samples included the realization
165 of both N₂ and CO₂ adsorption isotherms at 77 K and 273 K respectively, in order to investigate
166 all the dimensional ranges of AC porosity.

167 The N₂ adsorption isotherms, previously reported by Silvestre-Albero and co-workers³⁶,
168 showed that all the AC samples are mainly microporous with a narrow knee at low relative
169 pressure (Type I isotherms). Consequently, since it is generally accepted that CO₂ adsorption
170 occurs by a micropore filling mechanism^{28,37,38}, pore size distribution (PSD) is expected to play a
171 crucial role in determining CO₂ adsorption performances of the investigated AC samples.

172 In Figure 1, the PSD of all the AC samples, as derived from N₂ adsorption isotherms by
173 application of the QSDFT (Quenched Solid Density Functional Theory), are depicted.

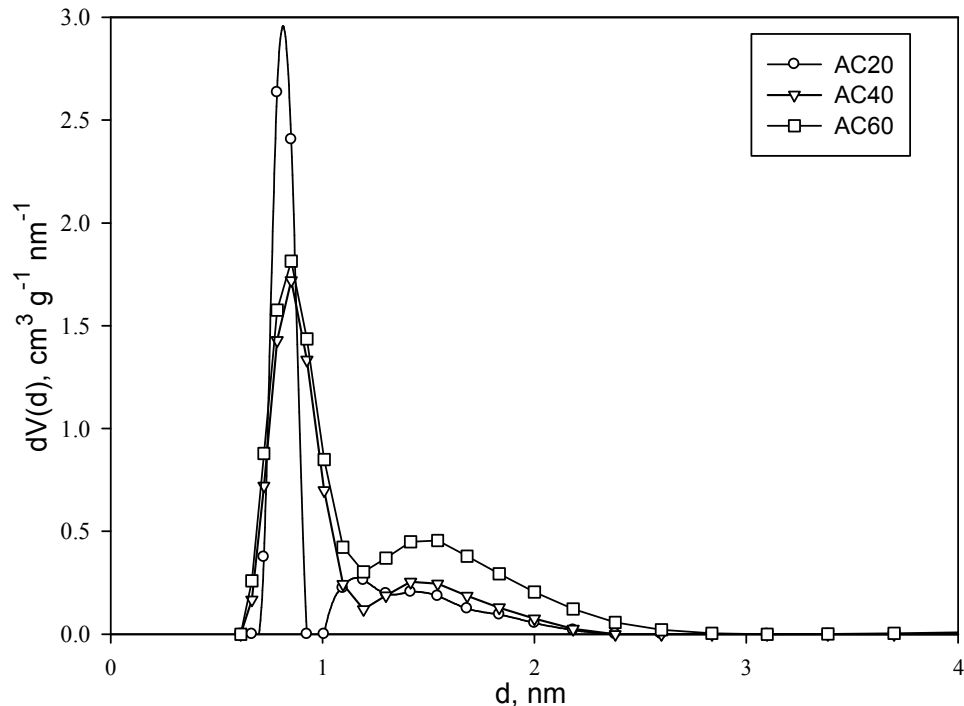
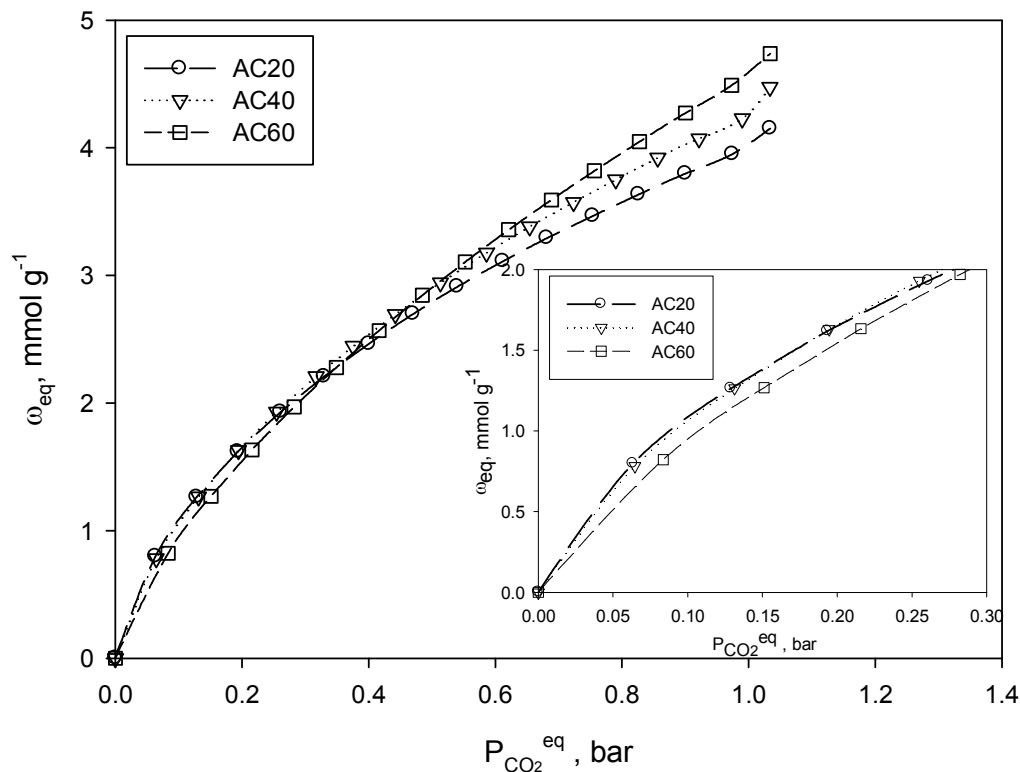


Figure 1. Pore size distribution of AC20, AC40 and AC60 samples obtained by QSDFT method (slit-shape equilibrium model) applied to N₂ adsorption isotherm at 77 K.

As it can be observed, the AC20 sample has the narrower PSD, mostly included in the range of narrow micropores (pore diameter < 10 Å). Differently, AC40 and AC60 samples have lower narrow micropore contribution, with a distribution shifted towards micropores of higher dimensions. In addition, AC60 sample shows a somewhat higher contribution of mesopores with respect to AC40 and, more, to AC20.

The analysis of the pertinent literature showed that microporous carbon materials with pores less than 1 nm are considered as the most suitable for CO₂ capture at ambient temperature and pressure^{13,26,30,39}. Hence, in order to deepen the investigation of smaller pore sizes and their

186 effect on CO₂ adsorption, CO₂ adsorption isotherms at 273 K were realized for all the AC
 187 samples and reported in Figure 2.



188
 189 **Figure 2.** CO₂ adsorption isotherms at 273 K for AC20, AC40 and AC60 samples. The
 190 inset graph represent the magnification of the 0-0.3 bar region.

191
 192 All the AC samples exhibit the expected isotherm shape and the adsorption capacity
 193 monotonically increases with CO₂ pressure and an asymptotic value is not reached in the
 194 investigated range.

195 All the parameters deriving from N₂ and CO₂ porosimetric analyses commonly adopted to
 196 fully characterize the textural properties of the AC samples are reported in Table 1.

197
 198

Sample	N ₂ adsorption, 77 K			CO ₂ adsorption, 273 K	
	S _{BET}	V _o	V _{meso}	V _t	V _n
	(m ² /g)	(cm ³ /g)	(cm ³ /g)	(cm ³ /g)	(cm ³ /g)
AC20	1253	0.46	0.07	0.53	0.36
AC40	1448	0.54	0.09	0.63	0.40
AC60	1983	0.70	0.23	0.93	0.45

Table 1. Textural parameters of AC20, AC40 and AC60 samples derived from N₂ and CO₂ adsorption isotherms at 77 K and 273 K, respectively

The application of the DR equation to N₂ and CO₂ isotherms allowed determining that a higher activation time resulted in both higher micropore (V_o) and narrow micropore (V_n) volumes, the increase of the former being more relevant. Coherently, also the BET surface area increased with the activation time, and the contribution of mesopores (V_{meso}) became significant only for AC60 sample, as already deduced by PSD analysis. A comparative analysis of the data reported in Table 1 shows that AC60 has the highest micropore volume (V_o), but AC20 has the highest fraction of narrower micropore (calculated as V_n/V_t ratio), as previously observed in Figure 1. Moreover, it can be stated that the activation treatment with CO₂ determines the opening of new micropores coupled with the broadening of the porosity, as testified by the increasing difference between micropores (V_o) and narrow micropores (V_n) as a consequence of a higher burn-off with activation time^{13,36}.

The results obtained so far would drive to the conclusion that AC60 is the most suitable sample for CO₂ adsorption. In fact, a higher micropore and narrow micropore contribution is commonly believed as a condition for the individuation of the sorbent with highest CO₂

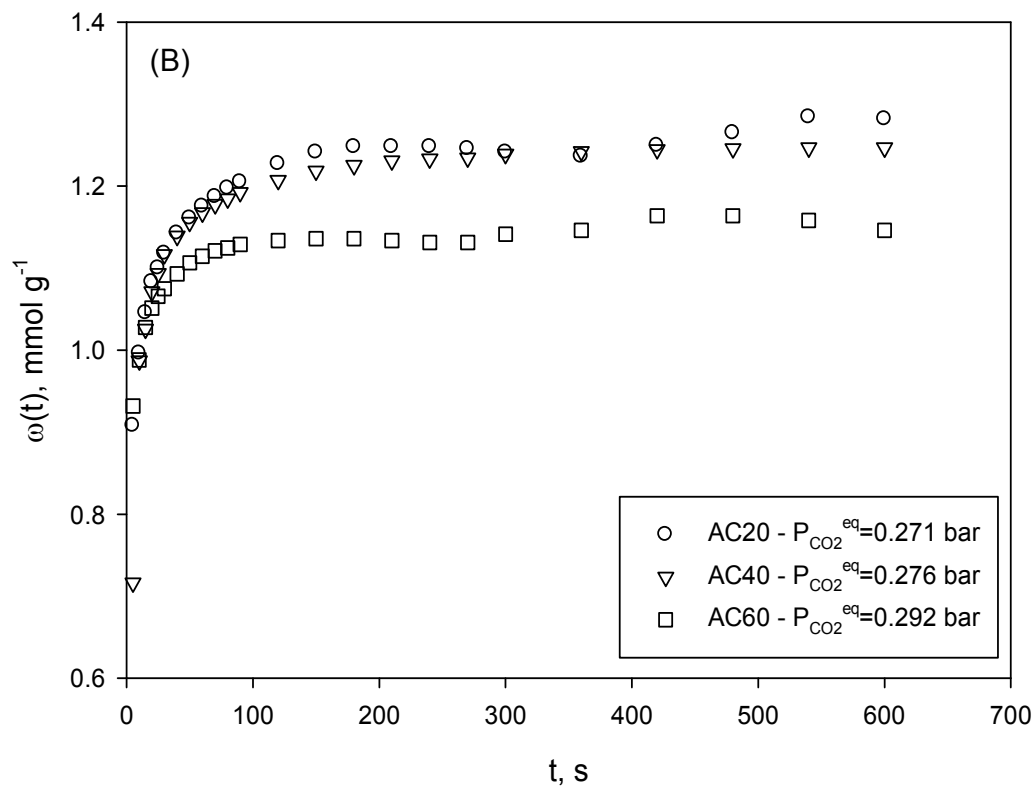
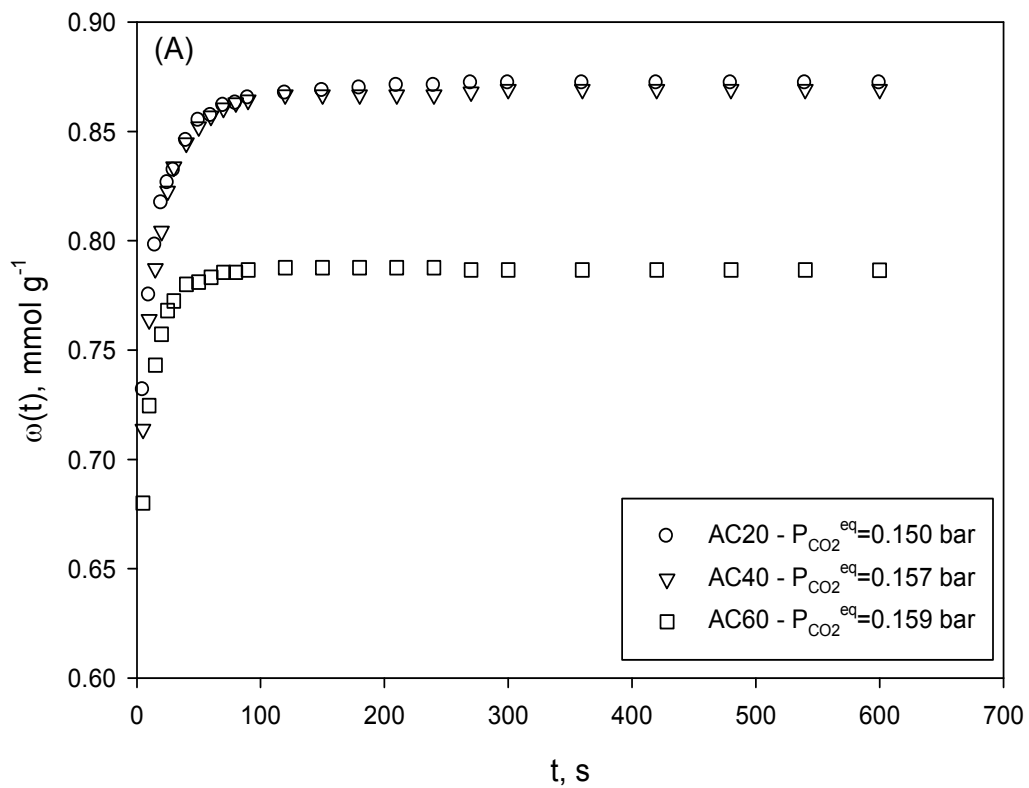
1
2
3 217 adsorption capacity (ω_{eq}). As a matter of fact, this result is always verified as long as CO₂
4
5 218 pressure assumes values equal to 1 bar^{13,19,26,30,31}. Coherently, data reported in Figure 2 confirms
6
7
8 219 that for a CO₂ pressure of 1 bar a monotonic ranking $\omega_{\text{eq}}(\text{AC60}) > \omega_{\text{eq}}(\text{AC40}) > \omega_{\text{eq}}(\text{AC20})$ exists.
9
10 220 However, it is interesting to observe that for a CO₂ pressure < 0.3 bar, the ranking is almost
11
12 221 inverted and becomes $\omega_{\text{eq}}(\text{AC20}) \approx \omega_{\text{eq}}(\text{AC40}) > \omega_{\text{eq}}(\text{AC60})$. This result suggests a different
13
14 222 energetic distribution of the active sites of the different AC samples, which favours the
15
16 223 adsorption capacity of AC20 and AC60 for low and high CO₂ pressure, respectively. An overall
17
18 224 analysis of the experimental results so far presented can be made following the Dubinin's
19
20 225 micropore filling theory. The high adsorption potential determined in narrow micropores, which
21
22 226 are mostly abundant in AC20 (cf. Figure 1) allows a more effective packing of CO₂ molecules
23
24 227 even at low adsorbate partial pressures, thus explaining the higher CO₂ adsorption capacity of
25
26 228 AC20 at low CO₂ pressures^{13,32,39}. The AC40 and AC60 samples show an almost similar
27
28 229 contribution of smaller micropores, even if the AC60 sample presents a sensibly higher
29
30 230 contribution of wider micropores and mesopores (as confirmed by data reported in Table 1),
31
32 231 these pores being favourably filled only at higher CO₂ partial pressures because of their lower
33
34 232 adsorption potential^{39,40}. On the basis of the reported PSD and from CO₂ adsorption data at 273
35
36 233 K (Figure 1), it can be deduced that the wider pores provide a higher contribution to CO₂
37
38 234 adsorption above a stated crucial value of CO₂ pressure.
39
40 235 These results assume an even greater importance when dealing with CO₂ capture from flue gas,
41
42 236 in which CO₂ concentration is always largely lower than 30%. However, in this step, the
43
44 237 analytical tests were performed in the fully automated manometric apparatus (cf. Section 2.1.)
45
46 238 with pure CO₂ at different pressure and at 273 K. Hence, in order to go into the effect of
47
48
49
50
51
52
53
54
55
56
57
58
59
60

1
2
3 239 temperature and CO₂ partial pressure further investigations were carried out in different
4
5
6 240 experimental conditions and reported in the following sections.
7

8 241

9
10 242 *3.2. CO₂ adsorption kinetics in batch system*
11

12
13 243 In order to extend the field of investigation of CO₂ adsorption onto the synthesized AC
14
15 244 samples, new experimental runs were carried out at 293 K in a manometric apparatus. To this
16
17 245 aim, kinetic batch tests were realized with pure CO₂ and for two different initial CO₂ pressure (
18
19
20 246 $P_{CO_2}^0$) levels, namely 0.25 and 0.42 bar. The results are depicted in Figure 3A and 3B,
21
22
23 247 respectively. It is worth to observe that the batch character of these tests leads to a variable CO₂
24
25 248 final equilibrium pressure which depends mainly on CO₂ equilibrium adsorption capacity, but
26
27
28 249 also on slight variations in the initial pressure and in the mass of the adsorbent charged into the
29
30 250 apparatus. Hence, for the sake of completeness, in Figure 3A-3B, the CO₂ equilibrium pressure (
31
32
33 251 $P_{CO_2}^{eq}$) was reported for each experimental run.
34
35
36
37
38
39
40
41
42
43
44
45
46
47
48
49
50
51
52
53
54
55
56
57
58
59
60



254 **Figure 3.** Pure CO₂ batch adsorption tests on AC samples at (A) $P_{CO_2}^0 = 0.25$ and (B) $P_{CO_2}^0 =$
 255 0.42 bar. T= 293 K; adsorbent dose: 0.2±0.01 g

257 From Figure 3 it can be observed that, for both the CO₂ initial pressures investigated, CO₂
 258 adsorption rate is higher for AC60, as testified by the lowest time taken to reach the final
 259 equilibrium adsorption capacity; on the other hand, differences between AC20 and AC40 are
 260 very slight. In Table 2, the equilibrium times (t_{eq}), as derived from experiments reported in
 261 Figure 3, are summarized:

	AC20	AC40	AC60
$t_{eq} (P_{CO_2}^0 = 0.25 \text{ bar}), \text{ s}$	210	180	90
$t_{eq} (P_{CO_2}^0 = 0.42 \text{ bar}), \text{ s}$	420	360	180

263
 264 **Table 2.** Comparison between equilibrium time (t_{eq}) values obtained from batch adsorption
 265 tests for AC20, AC40 and AC60 at different CO₂ initial pressure ($P_{CO_2}^0$)

267 These results reflect the mesopore content of the AC samples, highest for AC60 and
 268 comparable for AC40 and AC20, which is commonly believed to exert a significant influence on
 269 CO₂ adsorption rate^{13,32}. Moreover, the experimental results clearly demonstrate that in both the
 270 investigated experimental conditions AC60 has the lowest adsorption capacity while AC20
 271 displays comparable (Figure 3A) or slightly better (Figure 3B) CO₂ removal performances at
 272 equilibrium, with respect to AC40. However, a rigorous analysis should take into account also

1
2
3 273 the differences in equilibrium pressure, which allows considering AC20 favoured with respect to
4
5
6 274 AC40 also at lowest equilibrium pressure (Figure 3A). Hence, for the two tests conducted at CO₂
7
8 275 partial pressure <0.3 bar and T=293 K the new ranking of adsorption capacity is
9
10 276 $\omega_{eq}(AC20) > \omega_{eq}(AC40) > \omega_{eq}(AC60)$. A comparison with the adsorption isotherm at T=273 K
11
12 277 (Figure 2), equally realized with pure CO₂, confirms the exothermic character of CO₂ adsorption
13
14
15 278 (as expected the amount adsorbed is lower at 293 K for all samples) but leads to a further
16
17 279 important conclusion. An increase in temperature determines a reduction of the pore size
18
19
20 280 diameter active towards CO₂ adsorption; in fact, at 293 K, the AC20 sample shows the highest
21
22 281 difference in adsorption capacity with respect to AC40 and AC60 whereas these differences
23
24 282 decrease at 273 K. This result is consistent with the experimental findings reported by Zhang and
25
26 283 co-workers⁴¹ which observed that at higher temperature stronger adsorption potentials, as those
27
28 284 related with pore of smaller dimension, are required to avoid the adsorbate escaping from pores
29
30
31 285 (due to their higher kinetic energy). It can be concluded that narrow micropores play a more
32
33
34 286 relevant role at 293 K, with respect to 273 K, and low CO₂ pressures in determining higher
35
36 287 pollutant capture performances for AC20 sorbent.

38
39 288

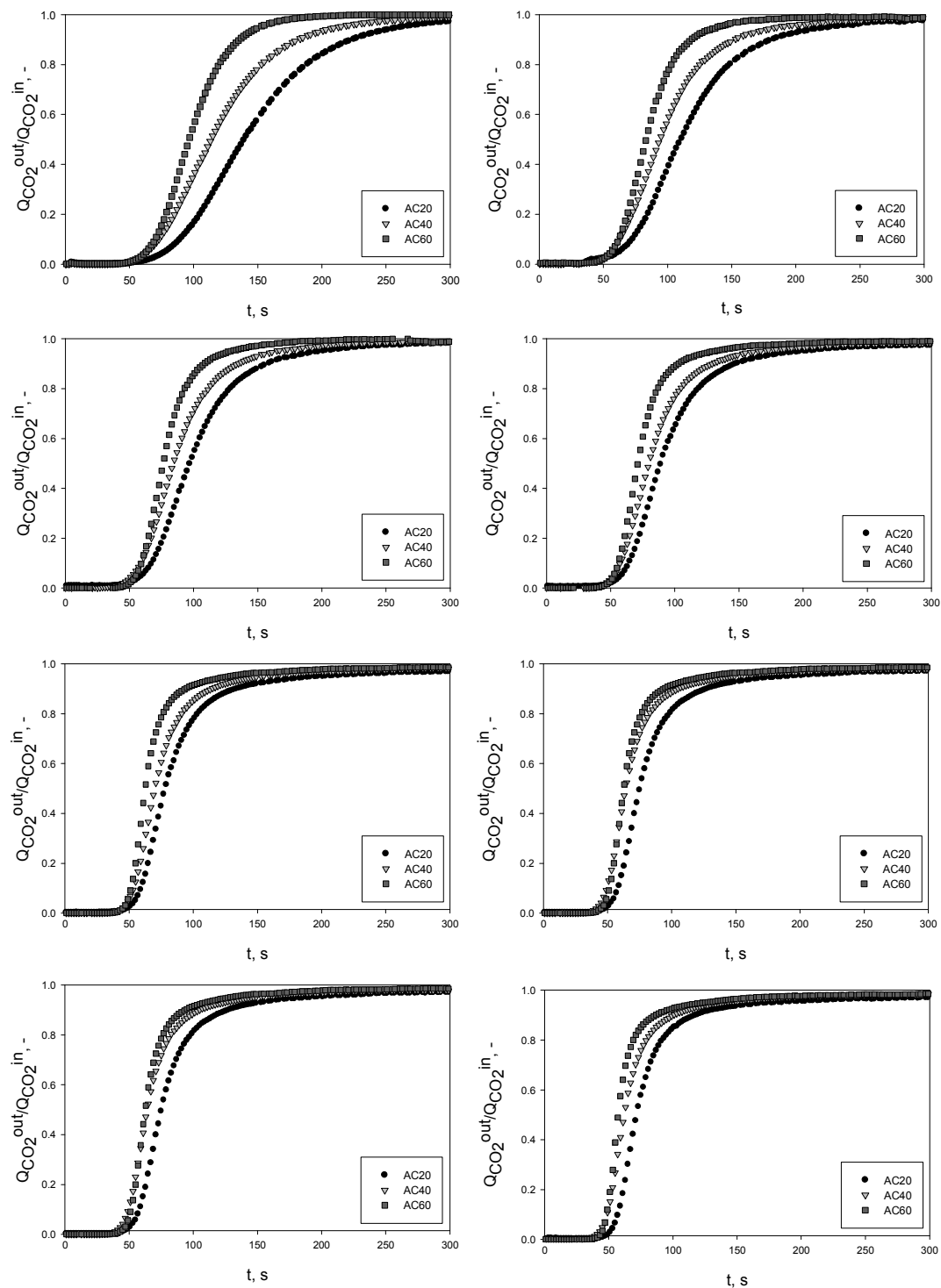
41 289 *3.3. CO₂ adsorption in dynamic system*

42
43 290 The above experimental results highlighted the substantial effect of temperature and CO₂
44
45
46 291 pressure on adsorption capacity of the investigated series of AC. In particular, the inversion of
47
48 292 performance ranking observed for a pressure < 0.3 bar drives to further investigations in this
49
50
51 293 range of pressures, which is consider of great interest because it includes those typical of a post-
52
53 294 combustion CO₂ capture treatment. The new experimental runs were performed at T= 293 K in a
54
55
56
57
58
59
60

1
2
3 295 dynamic system represented by a fixed-bed column, in which a model flue-gas composed by
4
5
6 296 CO₂+N₂ was fed.

7
8 297 The breakthrough profiles of CO₂ on AC20, AC40 and AC60 obtained at different CO₂
9
10 298 concentration in the feed (range 1-15% by vol.) are depicted in Figures 4 (A)-(H).

11
12
13 299
14
15
16
17
18
19
20
21
22
23
24
25
26
27
28
29
30
31
32
33
34
35
36
37
38
39
40
41
42
43
44
45
46
47
48
49
50
51
52
53
54
55
56
57
58
59
60



300
301 **Figure 4.** Breakthrough curves of CO₂ adsorption on AC20, AC40 and AC60 at different
302 CO₂ concentration in the feed (balance N₂). A) 1%; B) 3%; C) 5%; D) 7%; E) 9 %; F) 11%; G)
303 13%; H) 15%. T= 293 K, P=1 bar.

1
2
3 304 The analysis of the dynamic adsorption patterns reveals that for all the investigated CO₂
4
5 305 concentrations, AC60 shows the steeper curves and, hence, a faster CO₂ adsorption. This result is
6
7
8 306 consistent with the results derived from the batch tests carried out in the manometric apparatus
9
10 307 and can be ascribed to the wider pore dimension in the PSD of this sample (cf. Figure 2 and
11
12 308 Table 1). In addition, the kinetic adsorption profiles of AC40 and AC60 sorbents practically
13
14
15 309 overlap up to $Q_{\text{CO}_2}^{\text{out}}(t)/Q_{\text{CO}_2}^{\text{in}} \approx 0.1$, while a general smaller slope of the sigmoid is observed for
16
17
18 310 AC20, likely due to a higher narrow micropore contribution. Moreover, for all the AC samples,
19
20 311 an increase in CO₂ concentration fed to the column results in steeper breakthrough curves,
21
22 312 possibly related to faster mass transfer phenomena taking place at higher driving force^{32,42}.

23
24
25 313 The differences in mass transfer rates can be better evaluated by introducing a time parameter
26
27 314 $\Delta\tau=t_{0.7}-t_{0.1}$ (with $t_{0.1}$ and $t_{0.7}$ being the time for which $Q_{\text{CO}_2}^{\text{out}}(t)/Q_{\text{CO}_2}^{\text{in}}=0.1$ and 0.7, respectively)
28
29
30 315 which is related to the slope of the linear part of the sigmoid: the smaller this parameter the
31
32 316 steeper the breakthrough curve and consequently the faster the adsorption kinetics. The values of
33
34
35 317 $\Delta\tau$ derived from the kinetic patterns for AC 20, 40 and 60 are listed in Table 3.

36
37 318
38
39
40
41
42
43
44
45
46
47
48
49
50
51
52
53
54
55
56
57
58
59
60

	AC20	AC40	AC60
$\Delta\tau$ (CO ₂ :1%), s	77	64	40
$\Delta\tau$ (CO ₂ :3%), s	60	49	33
$\Delta\tau$ (CO ₂ :5%), s	47	40	26
$\Delta\tau$ (CO ₂ :7%), s	41	36	23
$\Delta\tau$ (CO ₂ :9%), s	35	30	21
$\Delta\tau$ (CO ₂ :11%), s	31	28	19
$\Delta\tau$ (CO ₂ :13%), s	28	26	16
$\Delta\tau$ (CO ₂ :15%), s	25	24	15

319

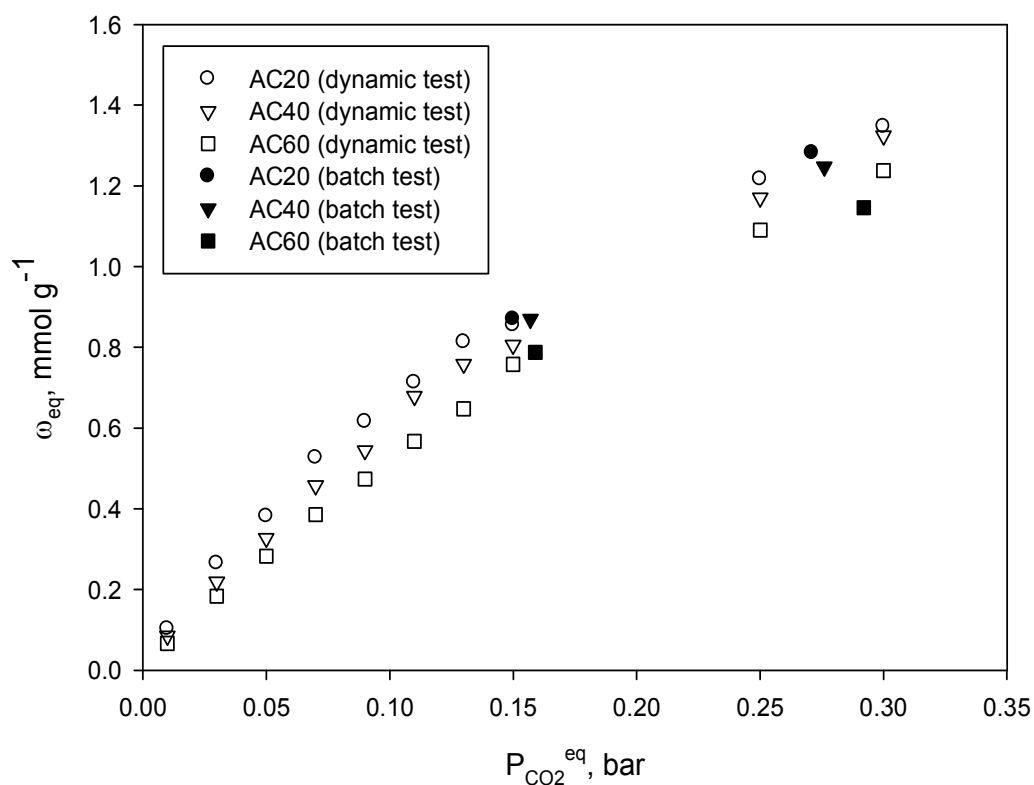
320 **Table 3.** Comparison between $\Delta\tau$ values obtained from dynamic adsorption tests for AC20,
 321 AC40 and AC60 at different CO₂ concentration in the feed

322

323 Results confirm a significantly faster adsorption for AC60 for all CO₂ concentrations,
 324 while they allow highlighting that the differences between AC20 and AC40 tend to reduce when
 325 the CO₂ initial concentration increases and become negligible when it approaches the maximum
 326 investigated value (15%). For example, at 15% CO₂ in the feed, $\Delta\tau = 15, 24$ and 25 s for AC 60,
 327 40 and 20 respectively. Even if the kinetic differences between AC20 and AC40 are not so
 328 marked, particularly at higher pollutant concentration, the CO₂ capture process is generally
 329 slightly slower for AC20, if the time needed to reach equilibrium is considered. This result fully
 330 confirms the outcomes derived from the batch kinetic tests (Figure 3) and it testifies the perfect
 331 integration between these two analytical tests in the analysis of CO₂ adsorption on AC samples.

Further indications about the kinetic can be drawn out from the evaluation of the breakpoint times t_b , defined as the time for which $Q_{CO_2}^{out}(t)/Q_{CO_2}^{in}=0.05$. The highest values shown by AC20, coupled with a more gentle slope, proves that in the investigated experimental conditions, this sample has the highest CO₂ adsorption capacity, as discussed in the following.

The experimental data obtained on the dynamic apparatus were processed according to Eq. (1), in order to obtain useful thermodynamic indications about the behaviour of AC samples in the investigated conditions. Figure 5 depicts the adsorption isotherms obtained at 293 K in terms of molar equilibrium adsorption capacity as a function of CO₂ equilibrium partial pressure $P_{CO_2}^{eq}$.



340
341 **Figure 5.** CO₂ adsorption isotherms on AC20, AC40 and AC60 as a function of CO₂
342 partial pressure (balance N₂). T=293 K and P=1 bar.
343

1
2
3 344 Experimental data clearly show that, in all the range of the investigated CO₂ partial pressure,
4
5 345 the ranking of adsorption capacity is $\omega_{\text{eq}}(\text{AC20}) > \omega_{\text{eq}}(\text{AC40}) > \omega_{\text{eq}}(\text{AC60})$. In particular, for a
6
7 346 typical flue gas composition (i.e. CO₂ partial pressure ~ 0.15 bar) the adsorption capacity
8
9 347 resulted to be 0.855, 0.806 and 0.758 mmol g⁻¹, respectively for AC20, AC40 and AC60. The
10
11 348 experimental error of this series of data is always included in a $\pm 5\%$ range, so that the observed
12
13 349 ranking cannot be altered. It is worth to observe that the ranking is confirmed also in an extended
14
15 350 range of CO₂ partial pressure (with respect to data reported in Figure 4). More interestingly, this
16
17 351 extension allowed to compare the data obtained in the dynamic apparatus with the homologous
18
19 352 data obtained in the batch apparatus, whose results were previously reported in Figures 3. To this
20
21 353 aim, CO₂ equilibrium adsorption data as derived from batch tests were also included in Figure 5.
22
23 354 A very good matching can be observed in terms of CO₂ adsorption capacity ranking, even if the
24
25 355 different experimental conditions adopted for the two series of data did not allow a punctual
26
27 356 comparison. Notwithstanding, it can be asserted with great confidence that the adsorption of N₂
28
29 357 on the synthesized AC samples can be considered as negligible. In fact, for each AC sample,
30
31 358 pure CO₂ adsorption data (batch series) and CO₂+N₂ adsorption data (dynamic series) almost lies
32
33 359 on the same adsorption isotherm. This result has very important implications in terms of practical
34
35 360 utilization of these AC samples in a post combustion treatment of a real flue gas, since the
36
37 361 competition of N₂ could seriously diminish CO₂ adsorption, affecting the efficiency of the
38
39 362 process. However, it has to be underlined that typical flue-gas compositions include the presence
40
41 363 of water, NO_x, SO_x and other contaminants which, despite of their low concentrations, can
42
43 364 significantly influence CO₂ adsorption. Summarizing the considerations drawn from batch and
44
45 365 dynamic adsorption tests at 293 K, it can be asserted that fixed bed experiments allow an
46
47 366 accurate and simultaneous evaluation of both thermodynamic capture capacity and of the
48
49
50
51
52
53
54
55
56
57
58
59
60

1
2
3 367 dynamic response of the gas-solid system, with associated time-saving advantages for the proper
4
5 368 selection of an activated carbon able to remove CO₂ from flue-gas under low operating pressure
6
7
8 369 (<0.15 bar). Contextually, data from Figure 4 permit to consider AC20 as a better sorbent for
9
10 370 practical application in large-scale adsorption unit aimed at mitigating CO₂-deriving global
11
12 371 warming effect because, despite its slower adsorption kinetics, it showed a higher equilibrium
13
14 372 adsorption capacity and a greater breakpoint time, hence it allows keeping CO₂ concentration at
15
16 373 a lower level for higher operating time with respect to AC40 and AC60 sorbents.
17
18
19

20 374 Finally, an overall evaluation of the experimental results obtained in this work drives to the
21
22 375 conclusion that the ranking observed in terms of CO₂ equilibrium adsorption capacity at 293 K
23
24 376 (Figure 5) is not in line with the ranking observed for micropore and narrow micropore volumes
25
26 377 (Table 1), for which AC60 results favoured. However, this evidence, apparently in contrast with
27
28 378 the results reported in the literature on similar experimentations, must be evaluated together with
29
30 379 the particular porous structure of the AC samples, which determines a combined dependence of
31
32 380 CO₂ adsorption capacity both on CO₂ partial pressure and temperature. In fact, the determination
33
34 381 of narrow micropore volume from CO₂ adsorption isotherm at 273 K (Figure 1) is made by
35
36 382 considering the cumulative contribution corresponding to the entire CO₂ pressure range (0-1
37
38 383 bar). In these conditions, AC60 showed the highest CO₂ capture performances and, coherently,
39
40 384 the highest narrow micropore volume. Conversely, until a CO₂ partial pressure <0.3 bar, AC20
41
42 385 showed the highest CO₂ adsorption capacity, also confirmed by experimental data realized at 293
43
44 386 K (Figure 3 and 5). Hence greater energetic interactions are determined by a higher adsorption
45
46 387 potential, likely due to a narrower PSD shifted to narrow micropores. It is interesting to remark
47
48 388 that these results were confirmed by comparing batch and dynamic data, realized in different
49
50 389 experimental devices. Therefore, this work allowed determining the importance of a combined
51
52
53
54
55
56
57
58
59
60

1
2
3 390 application of different techniques (i.e. batch and dynamic tests) for a thorough comprehension
4
5 391 of CO₂ adsorption on activated carbons and, in particular, for its practical application to the
6
7
8 392 treatment of a flue gas in its typical conditions of temperature, pressure and CO₂ concentration.
9
10
11 393

12 13 394 **4. Conclusions**

14
15 395 The assessment of CO₂ adsorption capacity on a series of three different activated carbons,
16
17 396 obtained from olives stones by physical and chemical activation at three different times i.e. 20,
18
19
20 397 40 and 60 hours, was experimentally carried out by a combination of batch and dynamic tests.
21

22 398 Preliminarily, a textural characterization of the samples (named AC20, AC40 and AC60)
23
24 399 showed a monotonic increase of both the micropore and ultramicropore volume with the
25
26
27 400 activation time, even if for CO₂ partial pressure lower than 0.3 bar the ranking for CO₂
28
29 401 adsorption capacity at 273 K is inverse, i.e. $\omega_{eq}(AC20) > \omega_{eq}(AC40) > \omega_{eq}(AC60)$. In order to
30
31 402 deeper investigate the relationship between textural properties and CO₂ capture performances,
32
33
34 403 kinetic and thermodynamic CO₂ adsorption tests were carried out at 293 K both in a batch
35
36 404 apparatus (pure CO₂ tests) and in a dynamic apparatus, represented by a lab-scale fixed-bed
37
38
39 405 column (CO₂+N₂ tests). In both the series of experiments, a very good agreement between
40
41 406 homologous experimental results was observed, which allowed considering as negligible N₂
42
43 407 adsorption on all the AC samples. For CO₂ pressure <0.3 bar, the AC60 showed the lowest
44
45
46 408 adsorption capacity but the fastest mass transfer phenomena, likely due to a remarkable greater
47
48 409 contribution of mesopores and a wider micropore size distribution. Conversely, the AC20 sample
49
50 410 exhibited the highest CO₂ adsorption capacity likely due to a greater contribution of smaller
51
52
53 411 pores in the ultramicropore range. Interestingly, the ranking of CO₂ adsorption capacity in
54
55 412 experimental conditions typical of a flue gas resulted to be $\omega_{eq}(AC20) > \omega_{eq}(AC40) > \omega_{eq}(AC60)$.
56
57
58
59
60

1
2
3 413 This ranking does not reflect the ranking observed in terms of ultramicropore volume
4
5 414 ($V_n(\text{AC60}) > V_n(\text{AC40}) > V_n(\text{AC20})$) determined by pure CO₂ isotherm at 273 K, but it is
6
7
8 415 coherent with the adsorption capacity displayed by all the AC samples at 273 K in
9
10 416 correspondence of a CO₂ pressure < 0.3 bar. Finally, this result highlights the importance of a
11
12 417 deeper analysis of adsorption data for the determination of the factor affecting CO₂ adsorption
13
14 418 performances. The different pore size distributions of the AC samples and in particular the
15
16 419 higher contribution of ultramicropores observed for AC20 sample play a major role in
17
18 420 determining a stronger interaction energy with CO₂ molecules at higher temperature and lower
19
20 421 CO₂ partial pressure.
21
22
23
24
25 422

26 27 423 **References**

- 28
29
30 424
- 31
32 [1] Yang, H.; Xu, Z.; Fan, M.; Gupta, R.; Slimane, R.; Bland, A.; Wright, I. Progress in carbon
33 dioxide separation and capture: A review. *J. Environ. Sci.* **2008**, *20*, 14-27.
 - 34
35 [2] Figueroa, J.; Fout, T.; Plasynski, S.; McIlvried, H.; Srivastava, R. Advances in CO₂ capture
36 technology-The U.S. Department of Energy's Carbon Sequestration Program. *Int. J. Greenh.*
37 *Gas Con.* **2008**, *2*, 9-20.
 - 38
39 [3] I. E. A. (IEA). Energy Technology Perspectives. **2010**. [Online]. Available:
40 <http://www.iea.org/techno/etp/etp10/English.pdf>.
 - 41
42 [4] Strube, R.; Manfrida, G. CO₂ capture in coal-fired power plants-Impact on plant
43 performance. *Int. J. Greenh. Gas Con.* **2011**, *5*, 710-726.
 - 44
45 [5] Brüder, P.; Svendsen, H. Capacity and kinetics of solvents for post-combustion CO₂ capture.
46 *Energy Procedia* **2012**, *23*, 45-54.
 - 47
48 [6] Herzog, H.; Meldon, J.; Hatton, A. Advanced post-combustion CO₂ capture. *Report*
49 *prepared for the Clean Air Task Force*, [Online]. Available:
50 <http://web.mit.edu/mitei/research/reports.html>, 2009.
 - 51
52
53
54
55
56
57
58
59
60

- 1
2
3
4 [7] Choi, S.; Drese, J.; Jones, C. Adsorbent materials for carbon dioxide capture from large
5 anthropogenic point sources. *ChemSusChem* **2009**, *2*, 796-854.
6
7 [8] Samanta, A.; Zhao, A.; Shimizu, G.; Sarkar, P.; Gupta, R. Post-combustion CO₂ capture
8 using solid sorbents: A review. *Ind. Eng. Chem. Res.* **2012**, *51*, 1438-1463.
9
10 [9] Abanades, J.; Rubin E.; Anthony, E. Sorbent cost and performance in CO₂ capture systems.
11 *Ind. Eng. Chem. Res.* **2004**, *43*, 3462-3466.
12
13 [10] Erto, A.; Lancia, A.; Musmarra, D. A Real Adsorbed Solution Theory model for competitive
14 multicomponent liquid adsorption onto granular activated carbon. *Micropor. Mesopor.*
15 *Mater.* **2012**, *154*, 45-50.
16
17 [11] Whaby, A.; Ramos-Fernández, J.; Martínez-Escandell, M.; Sepúlveda-Escribano, A.;
18 Silvestre Albero, J.; Rodríguez-Reinoso, F. High-surface-area carbon molecular sieves for
19 selective CO₂ adsorption. *ChemSusChem* **2010**, *3*, 974-981.
20
21 [12] Sanz, R.; Calleja, G.; Arenciba, A.; Sanz-Pérez, E.S. Development of high efficiency
22 adsorbents for CO₂ capture based on a double-functionalization method of grafting and
23 impregnation. *J. Mater. Chem. A* **2013**, *1(6)*, 1956-1962.
24
25 [13] Wahby, A.; Silvestre-Albero, J.; Sepúlveda-Escribano, A.; Rodríguez-Reinoso, F. CO₂
26 adsorption on carbon molecular sieves. *Micropor. Mesopor. Mater.* **2012**, *164*, 280-287.
27
28 [14] Liu, Y.; Wilcox, J. Effects of Surface Heterogeneity on the Adsorption of CO₂ in
29 microporous Carbons. *Environ. Sci. Technol.* **2012**, *46*, 1940-1947.
30
31 [15] Plaza, M.; Pevida, C.; Pis, J.; Rubiera, F. Evaluation of the cyclic capacity of low-cost
32 adsorbent for post-combustion CO₂ capture. *Energy Procedia* **2011**, *4*, 1228-1234.
33
34 [16] Gomes, V.; Yee, K. Pressure swing adsorption for carbon dioxide sequestration from
35 exhaust gases. *Sep. Purif. Technol.* **2002**, *28*, 161-171.
36
37 [17] Balsamo, M.; Budinova, T.; Erto, A.; Lancia, A.; Petrova, B.; Petrov, N.; Tsyntsarski, B.
38 CO₂ adsorption onto synthetic activated carbon: kinetic, thermodynamic and regeneration
39 studies. *Sep. Purif. Technol.* **2013**, *116*, 214-221.
40
41 [18] Sayari, A.; Belmabkhout, Y; Serna-Guerrero, R. Flue gas treatment via CO₂ adsorption.
42 *Chem. Eng. J.* **2011**, *171*, 760-774.
43
44 [19] Yang, R.; Liu, G.; Li, M.; Zhang, J.; Hao, X. Preparation and N₂, CO₂ and H₂ adsorption of
45 super activated carbon derived from biomass source hemp (*Cannabis sativa* L.) stem.
46
47
48
49
50
51
52
53
54
55
56
57
58
59
60

- 1
2
3
4
5
6
7
8
9
10
11
12
13
14
15
16
17
18
19
20
21
22
23
24
25
26
27
28
29
30
31
32
33
34
35
36
37
38
39
40
41
42
43
44
45
46
47
48
49
50
51
52
53
54
55
56
57
58
59
60
- Micropor. Mesopor. Mater.* **2012**, *158*, 108–116.
- [20] Shen, C.; Grande, C.; Li, P.; Yu, J.; Rodrigues, A. Adsorption equilibria and kinetics of CO₂ and N₂ on activated carbon beads. *Chem. Eng. J.* **2010**, *160*, 398-407.
- [21] Marsh, H.; Rodríguez-Reinoso, F. *Activated Carbon*, Elsevier Science & Technology Books: Amsterdam, 2006.
- [22] Ello, A. S.; de Souza, L. K.; Trokourey, A.; Jaroniec, M. Coconut shell-based microporous carbons for CO₂ capture. *Micropor. Mesopor. Mater.* **2013**, *180*, 280-283.
- [23] Vargas, D. P.; Giraldo, L.; Moreno-Piraján, J. C. CO₂ adsorption on granular and monolith carbonaceous materials. *J. Anal. Appl. Pyrol.* **2012**, *96*, 146–152.
- [24] Hao, W.; Björkman, E.; Lilliestråle, M.; Hedin, N. Activated carbons prepared from hydrothermally carbonized waste biomass used as adsorbents for CO₂. *Appl. Energ.* **2013**, *112*, 526-532.
- [25] Vargas, D.; Giraldo, L.; Moreno-Piraján, J. Activated carbon for CO₂ adsorption obtained through the chemical activation of African palm stone. *Adsorpt. Sci. Technol.* **2013**, *31(9)*, 845-858.
- [26] Lee, S. Y.; Park, S. J. Determination of the optimal pore size for improved CO₂ adsorption in activated carbon fibers. *J. Colloid Interface Sci.* **2013**, *389(1)*, 230–235.
- [27] Vargas, D.; Giraldo, L.; Erto, A.; Moreno-Piraján, J. Chemical modification of activated carbon monoliths for CO₂ adsorption. *J. Therm. Anal. Calorim.* **2013**, *114(3)*, 1039-1047.
- [28] Sevilla, M.; Parra, J.; Fuertes, A. Assessment of the role of micropore size and N-doping in CO₂ capture by porous carbons. *Appl. Mater. Interf.* **2013**, *5(13)*, 6360-6368.
- [29] Sun, N.; Sun, C.; Liu, H.; Liu, J.; Stevens, L.; Drage, T.; Snape, C. E.; Li, K.; Wei W.; Sun, Y. Synthesis, characterization and evaluation of activated spherical carbon materials for CO₂ capture. *Fuel* **2013**, *113*, 854-862.
- [30] Wickramaratne, N. P.; Jaroniec, M. Importance of small micropores in CO₂ capture by phenolic resin-based activated carbon spheres. *J. Mater. Chem. A* **2013**, *1*, 112-116.
- [31] Yin, G.; Liu, Z.; Liu, Q.; Wu, W. The role of different properties of activated carbon in CO₂ adsorption. *Chem. Eng. J.* **2013**, *230*, 133-140.
- [32] Balsamo, M.; Rodríguez-Reinoso, F.; Montagnaro, F.; Lancia, A.; Erto, A. Highlighting the role of activated carbon particle size on CO₂ capture from model flue gas. *Ind. Eng. Chem.*

- 1
2
3
4 *Res.* **2013**, *52*, 12183–12191.
- 5
6 [33] Dantas, T. L. P.; Luna, F. M. T.; Silva Jr., I. J.; de Azevedo, D. C. S.; Grande, C. A.;
7 Rodrigues, A. E.; Moreira, R. F. P. M. Carbon dioxide–nitrogen separation through
8 adsorption on activated carbon in a fixed bed. *Chem. Eng. J.* **2011**, *169*, 11-19.
- 9
10
11 [34] García, S.; Gil, M.; Martín, C.; Pis, J.; Rubiera, F.; Pevida, C. Breakthrough adsorption
12 study of a commercial activated carbon for pre-combustion CO₂ capture. *Chem. Eng. J.*
13 **2011**, *171*, 549-556.
- 14
15
16 [35] Yong, Z.; Mata, V.; Rodrigues, A. Adsorption of carbon dioxide on chemically modified
17 high surface area carbon-based adsorbents at high temperature. *Adsorption* **2001**, *7*, 41-50.
- 18
19
20 [36] Silvestre-Albero, A.; Silvestre-Albero, J.; Sepúlveda-Escribano, A.; Rodríguez-Reinoso, F.
21 Ethanol removal using activated carbon: Effect of porous structure. *Micropor. Mesopor.*
22 *Mater.* **2009**, *120*, 62–68.
- 23
24
25 [37] Garrido, J.; Linares-Solina, A.; Martín-Martinez, J.; Molina-Sabio, M.; Rodríguez-Reinoso,
26 F.; Torregrosa, R. Use of nitrogen vs carbon dioxide in the characterization of activated
27 carbons. *Langmuir* **1987**, *3*, 76-81.
- 28
29
30 [38] Martín-Martinez, J. M.; Torregrosa-Macia, R.; Mittelmeijer-Hazeleger, M. C. Mechanisms of
31 adsorption of CO₂ in the micropores of of activated anthracite. *Fuel* **1995**, *74*, 111-114.
- 32
33
34 [39] Casco, M.; Martínez-Escandell, M.; Silvestre-Albero, J.; Rodríguez-Reinoso, F. Effect of the
35 porous structure in carbon materials for CO₂ capture at atmospheric and high-pressure.
36 *Carbon* **2014**, *67*, 230-235.
- 37
38
39 [40] Cazorla-Amorós, D.; Alcañiz-Monge, J.; de la Casa-Lillo, M.; Linares-Solano, A. CO₂ as an
40 adsorptive to characterize carbon molecular sieves and activated carbons. *Langmuir* **1998**,
41 *14(16)*, 4589–4596.
- 42
43
44 [41] Zhang, Z.; Zhou, J.; Xing, W.; Xue, Q.; Yan, Z.; Zhuo, S.; Zhang Qiao, S. Critical role of
45 small micropores in high CO₂ uptake. *Phys. Chem. Chem. Phys.* **2013**, *15*, 2523-2529.
- 46
47
48 [42] Ruthven, D. *Principles of adsorption and adsorption processes*; John Wiley & Sons:New
49 York, 1984.
- 50
51

425

426